Rovibrational Crystal Field Splitting of Small Molecules Embedded in Solid Parahydrogen Matrix

Song Yan

A Thesis Submitted in Partial Fulfilment
of the Requirements for the Degree of
Master of Philosophy
in
Chemistry

Supervised by

Prof. Man-Chor Chan

June 2006

THESIS COMMITTEE

Supervisor:

Prof. Man-Chor Chan

Examining Broad:

Prof. Zhifeng Liu (Chairman)

Prof. Dominic Tak-Wah Chan

Prof. Man-Chor Chan

Prof. Allan Shi-Chung Cheung (External examiner)

ABSTRACT

In this thesis, the rovibrational crystal field splitting of heteronuclear diatomic molecules trapped in a hexagonal close-packed (*hcp*) solid parahydrogen (p-H_2) was studied theoretically from the first principles. The group theoretical treatments based on permutation-inversion group theory were worked out to study the symmetry of rovibrational wavefunctions, dipole moment, and optical selection rules. The energy correction of the rovibrational levels in the crystal field was calculated by considering the multipole-induced dipole interactions between the impurity molecule and the surrounding p-H_2 molecules. The relative intensities of the rovibrational transitions calculated using the Boltzemann distribution and Racah algebra were consistent with the results from group theory.

The theory was applied to the case of CO molecules trapped in the p-H_2 crystals. It was found that in this case the splitting was mainly due to quadrupole-induced dipole interaction. The crystal field splitting for the first few J manifolds were determined to be on the order of a few cm^{-1} using the explicit expression derived from our theory. A preliminary analysis of the experimental spectrum based on the predicted spectrum was also discussed.

Abstract of thesis entitled:

Rovibrational Crystal Field Splitting of Small Molecules Embedded in Solid ParaHydrogen Matrix

Submitted by Yan Song

for the degree of Master of Philosophy in Chemistry

at The Chinese University of Hong Kong in June 2006

中文摘要

本文鎚第一性原理著手，理論研究了異核雙原子分子孤立在六方密積結構(*hcp*)固態仲氫(p-H_2)中的振轉晶體場分裂。利用在置換－倒相群論基礎上發展的擴充群論，研究了雜質分子的振動－轉動波函數的對稱性，電偶極矩的對稱性以及光學選擇定則。通過考慮雜質分子和周圍仲氫分子之間的多極感生偶极相互作用，量化計算了晶體場中振轉能級的能量修正。同時發現，利用玻爾茲曼分布和拉卡代數計算所得的振轉能級躍遷相對强度和基於群論的結果是一致的。

應用以上理論，討論了在固態仲氫晶體場中摻雜一氧化碳分子的系統。在此系統中，晶體場分裂主要來自于四極感生偶極相互作用。基於我們的理論，精確計算了 J 低能級的晶體場分裂能量（量級在幾個 cm^{-1}）。此外，參照預測的理論光譜，對實驗光譜進行了初步的分析。

ACKNOWLEDGENTS

I wish to express my gratitude to my supervisor, Professor Man-Chor Chan, for his intelligent ideas, for his analytical guidance and for his many valuable comments and criticisms in every stages of this research.

I also want to acknowledge the extensive contributions of my fellow members in the Laboratory for Laser Spectroscopy: Shun-Hin Yeung instructed me in basic background and method in spectrum research. Kwok-Cheung Lo provided enthusiastic help on my classes. Fangyuan Han shared considerable brainpower with me. Lei Yan gave his helpful guide on software. Hailing Wang and Jun Liu made me several suggestions that more or less influenced the organization of this theory.

Above all, I would like to especially thank my family and all my friends for the invaluable and continuous encouragement and support.

TABLE OF CONTENTS

LIST OF FIGURES

LIST OF TABLES

CHAPTER 1

INTRODUCTION

1.1. Motivation

While intermolecular interactions and potentials have been known for years, our knowledge about them is still very limited. The interactions between molecules play important roles in many physical and chemical processes of matter. For instance, the process of phase transition is governed by the intermolecular interaction. Products and rates of chemical reactions are greatly affected by the relative orientation of the reacting molecules that are controlled by the long-range interactions among them. To date, the Lennard-Jones (6-12) isotropic potential is still the most commonly used model.[1] While isotropic intermolecular potential has been studied using *ab initio* calculations,[2-4] information on anisotropic intermolecular potential relies heavily on experimental data. High resolution spectroscopy of the van der Waals complexes (species formed by two molecules held by intermolecular interactions) using supersonic expansion has been established as a powerful means for studying intermolecular interactions. Nevertheless, the low concentration of complexes in the beam requires special detection technique.

Another approach to the issue is to study intermolecular interactions in the condensed phase. However, spectral transitions in the condensed phase often suffer

serious homogeneous and inhomogeneous broadening that smear out the detailed structure due to intermolecular interactions. Solid parahydrogen, as an exception, exhibits exceedingly narrow spectral width (~10-100MHz) that is comparable to those observed in the gas phase. Since the initial work by Welsh and coworkers, spectroscopic studies of solid hydrogen have been pursued for over four decades.[5,6] It was until the early 1980s that Hardy, Berlinsky, Harris, and their coworkers observed microwave transitions due to impurity molecules in solid parahydrogen exhibiting widths as sharp as 1MHz (HWHM, half-width at half-maximum).[7-12] The observation of the $\Delta J = 6$ (W-branch) transitions of p-H_2 in the infrared region by Okumura, Chan and Oka in the late 1980s[13,14] has renewed the interest in pursuing high resolution spectroscopy in the system of solid hydgrogen.[14]

Following the observation of the W transitions of p-H_2, high resolution spectra of a variety impurity species such as o-H_2, p-D_2, o-D_2, CO, CH_3, and CH_4 in p-H_2 crystal have been studied. [14-21] In addition, attempts at high resolution studies of ionic species in p-H_2 have also been reported.[22,23] These studies indicate that the applicability of p-H_2 as a matrix in studying intermolecular interactions of impurities through high resolution spectroscopy. On the other hand, the theoretical basis of the rovibrational fine structure of the impurity spectrum as a result of crystal field interaction has been sketchy. In this thesis, we will present a model, from the first principles, to account for the crystal field splitting of heteronuclear diatomic molecules in parahydrogen crystals by considering the long-ranged multipole interactions, which are considered the major interactions in the crystal.

1.2. Properties of Molecular Hydrogen

Hydrogen is the simplest and most fundamental molecule of all.[24] Due to its simplicity, H_2 has been an ideal system to test the high level structural calculations. The low molecular mass and the high binding energy of H_2 make it a potential candidate for energy source and storage due to its high per mass energy content. Extensive studies along this line have been actively pursued.[25-28] As the most abundant species in the universe, hydrogen also plays important roles in astrochemistry and the evolution of stars. Properties of hydrogen have been well documented in various aspects.[29-33] A list of its physical properties is given in TABLE 1. A brief review of the properties related to our study is given below.

Hydrogen molecules exist in two forms characterized by total nuclear spin (I) of the nuclei. Orthohydrogen (o-H_2) are species with $I = 1$ while parahydrogen (p-H_2) are species with $I = 0$. According to the Pauli principle,[34] o-H_2 molecules can only populate J = odd rotational levels while p-H_2 populate J = even levels. The conversion between *ortho* and *para* species is extremely slow (on the order of months) in the absence of catalysts. As a result, these two species behave as two different types of molecules and therefore named nuclear spin modifications. At room temperature, the ortho/para ratio of normal hydrogen is 3 to 1, resulted from the allowed projections of the nuclear spin quantum numbers. This ratio remains even when the gas is cooled to its triple point at ~14 K. Due to the large rotation constant of H_2, only $J = 0$ and $J = 1$ levels are thermally populated at a ratio of 1 to 3 at this temperature. In the presence of paramagnetic catalysts (such as APPACHI catalyst),[35] however, the ortho/para ratio reaches equilibrium at the surrounding temperature in

TABLE 1 Basic physical properties of hydrogen.

Molecular mass	2.0157 g/mol
Density	0.08988 g/L (0 °C, 101.325 kPa)
Boiling point	20.28 K
Melting point	14.01 K
Triple point	13.8033 K, 7.042 kPa
Critical temperature	32.19 K
Critical pressure	1.315 MPa
Critical density	30.12 g/L
Heat of vaporization	0.904 kJ/mol
Heat of fusion	0.117 kJ/mol
Heat capacity	28.836 J/(mol·K) (25 °C)
Dielectric strength	1.294
Volume resistivity	10^{19} (not constant)
Dielectric constant	1.25
Surface Tension	$1.93*10^{3}$ dynes/cm

seconds. This property allows the production of para-enriched hydrogen by simply controlling the temperature in the presence of catalysts. In experiments using para-enriched hydrogen, a in-line converter containing catalysts is often used in a temperature range between 14 and 20 K to obtain 99.8~99.996% of p-H_2.

As a homonuclear diatomic molecule, hydrogen has no dipole moment. On the other hand, the non-spherical electronic wavefunction gives rise to nonzero multipole moments. These multipole moments, although weak, play important roles in the observable rovibrational spectrum of hydrogen in high pressure regime and the condensed phases. The detailed theory to interpret these spectra can be found in a number of review articles.[35-38]

1.3. Properties of Solid Hydrogen

Solid hydrogen with two crystal structures, namely face-centered cubic (*fcc*) and hexagonal close-packed (*hcp*), is formed from molecular hydrogen depending on the growth conditions. Both structures correspond to the most efficient packing geometry. The *fcc* lattice is composed of a stacking of three hexagonal planes α, β, and γ with the lattice points of middle plane β being the inversion centers shown in FIG. 1. By comparison, the *hcp* lattice is composed of a stacking of two hexagonal planes α and β. They shift horizontally from each other as shown in FIG. 2. It has been reported that *hcp* structure is obtained when the solid is made from liquid while *fcc* structure is obtained when the solid is made from gas.[44] The nearest neighboring distance (R_0) in solid hydrogen is 3.793 Å, which is larger than that for most simple crystals.[40]

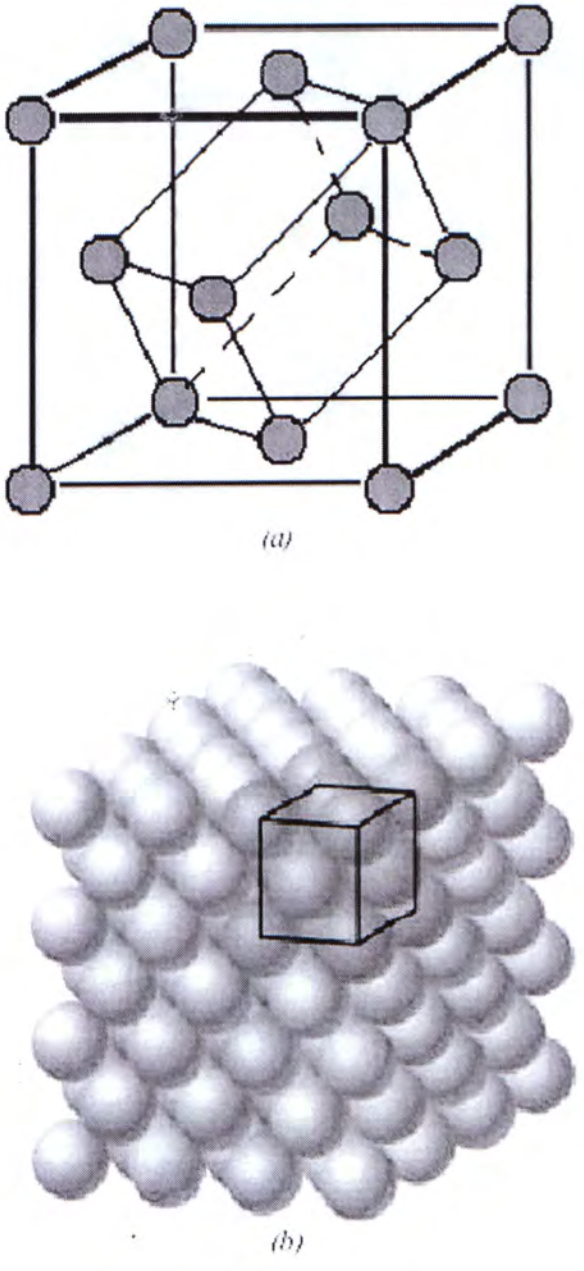

FIGURE 1 For the face-centered cubic (*fcc*) structure. (a) a reduced-sphere unit cell, and (b) an aggregate of many atoms.[39]

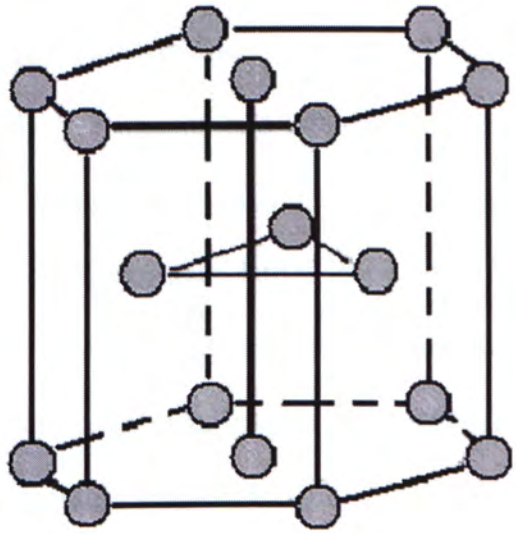

(a)

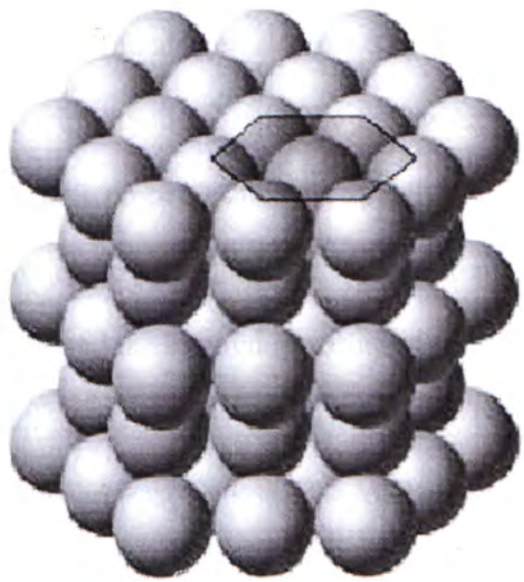

(b)

FIGURE 2 For the hexagonal close-packed (*hcp*) structure. (a) a reduced-sphere unit cell, and (b) an aggregate of many atoms. [39]

Solid hydrogen is the simplest molecular solid yet possesses a number of fascinating properties governed by quantum effects.[41] It has been known that molecules undergo nearly free rotation and vibration in p-H_2 as demonstrated in a number of spectroscopic studies. The weak interaction among molecules in the solid allows very large amplitude of zero-point lattice vibration (~ 20% of R_0) that makes it a "transitional quantum crystal".[42] The large intermolecular separation among hydrogen molecules in the solid gives rise to its softness and the extremely rich phases in the ultrahigh pressure regime. Rotational diffusion is another interesting quantum phenomenon due to resonance exchange of ortho/para hydrogen that is responsible for the equilibrium of spatial distribution of ortho and para hydrogen at cryogenic temperature. Most fundamental properties of solid hydrogen have been well summarized in a book by Souers[43] and in a review article by Silvera.[44] Here we just discuss the spectroscopic properties that are directly related to our study.

Since the first observation of the Raman spectrum of liquid hydrogen by McLennan and McLeod[45] and the infrared spectrum of solid hydrogen by Allin, Hare, and MacDonald,[46] hydrogen has been known to have vibrational and rotational degrees of freedom in the condensed phase. The rovibrational spectrum of solid H_2 is ascribed to the dipole induced by the multipole moments of the surrounding molecules. Van Kranendonk and his coworkers established a self-consistent theory to interpret the observed spectra including the transition frequencies, linewidths, and intensities based essentially on the multipole-multipole interactions in the solid. The details of the theoretical treatments have been summarized in a book by Van Kranendonk.[24]

The most remarkable observation is the extremely narrow linewidths in solid hydrogen as shown in the experimental work since the 1980s. The observation of the very sharp (~ 90 MHz HMWM) $J = 6 \leftarrow 0$ pure rotational transitions of solid p-H_2 with resolved M splitting due to the crystal field interactions indicated that solid H_2 is a unique system for applying high resolution spectroscopy to study intermolecular interactions.[13] Following this promising result, various vibrational and rotational transitions including $Q_v(0)$, $Q_1(1)$, $S_0(0)$, $U_0(0)$, $U_1(1)$,$W_0(0)$ and $W_1(0)$ transitions of host p-H_2 molecules as well as isotopic impurity species have been studied using high resolution infrared and stimulated Raman-gain spectroscopy. [14,15,35,47-51] It is interesting that intermolecular interactions on one hand give rise to the observable rovibrational spectrum, yet on the other hand are too weak to cause a fast relaxation and thus broaden spectral widths. While the quantitative interpretation of the observed linewidths is yet to be studied, there is little doubt from the observations that solid p-H_2 may be used as a matrix material for high resolution spectroscopy even though solid H_2 has not been considered an ideal matrix material due to its softness and high vapor pressure at cryogenic temperature.

The properties of solid hydrogen, on the other hand, present a unique environment to the matrix-isolated molecules to have nearly free rotation and vibration for high resolution spectroscopy. First of all, the nearest-neighboring intermolecular distance (3.793 Å) is much larger than the internuclear distance (0.741 Å) and the van der Waals radius (1.57 Å).[52] These distances allow guest molecules to occupy a lattice site without seriously disturbing the crystal structure. In addition, the rotational wavefunction of the J= 0 p-H_2 is spherically symmetric to give rise to a

nearly isotropic environment with very weak intermolecular interactions. This minimizes the angular-dependent intermolecular interactions resulting from electron overlap and dispersion, resulting in a long dephasing time of the excitation energy and narrow homogeneous linewidths. Finally, the very weak intermolecular interactions with relatively large zero-point lattice vibration lead to rapidly tunneling of hydrogen molecules between equivalent sites. This tunneling process is the basis for the self-annealing behavior observed in hydrogen crystals. As a result, the crystals are nearly free of defects and strains with excellent optical quality (even in the presence of trace impurities) to allow quantitative analysis of fine spectral features.

To date, a variety of chemical species in solid parahydrogen matrix have been studied by infrared (*IR*) spectroscopy following the work of CH_4 in *p*-H_2 crystal.[19-21] In most cases, the analysis of the spectra is still at a primitive stage. The theoretical studies of the high resolution spectra post challenging problems. As a starting point, a theoretical model to study the crystal field splitting of heteronuclear diatomic (AB) molecules in parahydrogen crystal has been developed. The selection rules and the rovibrational spectrum will also be discussed. In Chapter 2, the theoretical framework to account for the crystal field splitting of AB molecules in a hexagonal close-packed *p*-H_2 crystal will be established. The application of our theoretical model to the case of CO impurities in parahydrogen crystal will be discussed in Chapter 3. In Chapter 4, a brief discussion and concluding remark will be given. It is hoped that this work will provide a pilot study to predict the rovibrational spectrum from the first principles.

CHAPTER 2

THEORY

In this chapter, a theoretical framework for the quantitative analysis of the rotation-vibration spectra of heteronuclear diatomic (AB) molecules in a hexagonal close-packed (*hcp*) solid parahydrogen crystal will be constructed. We will consider the problem in two aspects based on symmetry consideration and numerical calculations. The former is a qualitative but rigorous approach providing insights of the problem while the latter is a quantitative but approximate approach providing numeric information with certain error/uncertainty.

In our consideration, each AB molecule is assumed to be well isolated and occupy a lattice site in a p-H_2 crystal with *hcp* structure. Each p-H_2 molecule is treated as a point mass with no internal structure. As shown in FIG. 3, the crystal environment exhibits the D_{3h} point symmetry. Because of the anisotropy in the surrounding, rovibrational levels of AB molecules are expected to split according to the orientation of the molecular axis, i.e. the projection quantum number M of the angular momentum J. The nature of the M splitting can be ascribed to the angle-dependent multipole-induced dipole interactions between the surrounding p-H_2 molecules and the central AB molecule. It has been known that p-H_2, as homonuclear diatomic molecules, possess no permanent dipole moment. Nevertheless, the multipole moments of order l (Q_l) of the central AB molecule (due to non-spherical

charge distribution) can polarize the surrounding p-H_2 molecules with polarizability tensor α to give rise to induced dipole moments. These induced dipole moments will interact with the multipole moments of the impurity molecule to lead to a correction in electrostatic interaction energy. This second-order interaction is weak but observable in the case of solid H_2 as revealed in the $W_0(0)$ transition.[13] In establishing the theoretical model, the group theoretical treatment will be discussed in Section 2.1, followed by numerical calculations of the crystal field splitting of rovibrational levels and multipole moments of AB based on the first principles in quantum mechanics in Section 2.2 and 2.3, respectively. Finally, the corresponding rovibrational spectrum with relative intensity will be discussed in Section 2.4.

2.1. Group Theory

The properties of a physical system are governed by its symmetry (invariance) properties. Based on symmetry considerations, one can classify energy levels and deduce selection rules for nonzero matrix elements of perturbation operators and transitions. Symmetry classification of molecular parameters (e.g. vibrational mode, molecular-fixed components of dipole and polarizability, etc.) as well as molecular wavefunctions has been well established. The construction of molecular symmetry group based on the feasible symmetry operations commuting with the molecular Hamiltonian has been extensively studied. The results are summarized in a book by Bunker and Jensen.[53] While the complete symmetry group of a molecule is composed of thousands of operations, only a small number of operations are feasible under certain experimental conditions and thus needed for the symmetry classification of

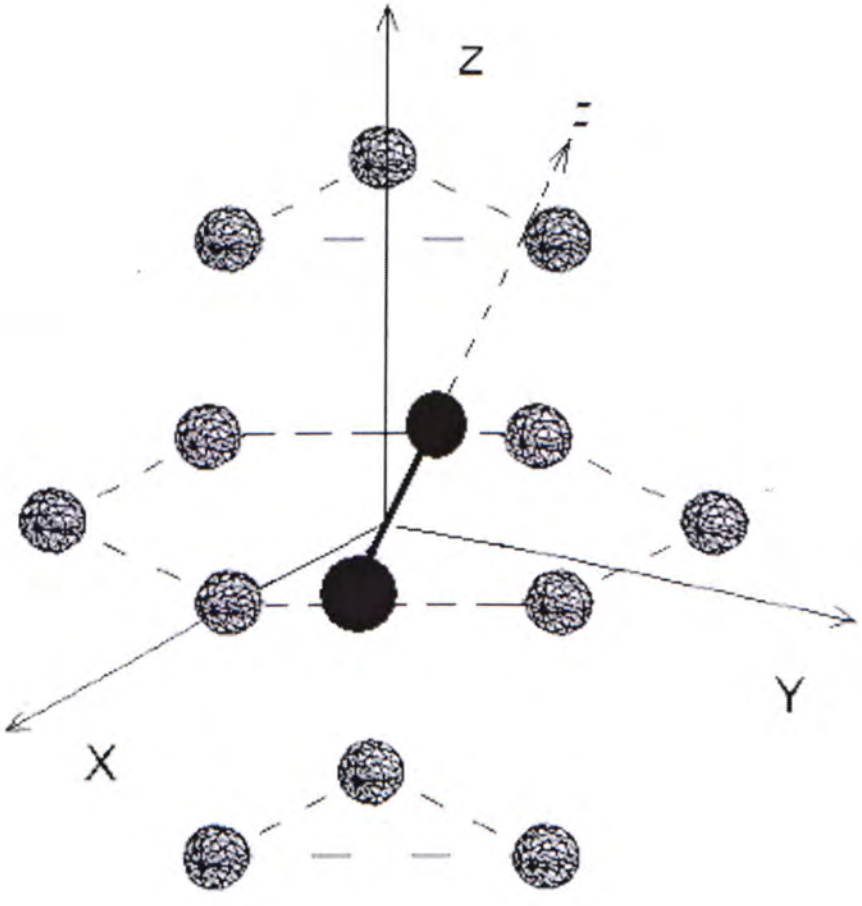

FIGURE 3 Crystal structure of an AB molecule trapped in the *hcp* crystal of *p*-H_2. Small empty circles indicate *p*-H_2 molecules and the filled circles indicate an AB molecule. In the crystal-fixed axis system, the crystal Z axis is perpendicular to the hexagonal plane and the XY axis is in the plane. In the molecule-fixed system, the C_∞^ϕ symmetry axis of the radical is taken as the z axis of the molecule AB and xy axis is in the plane perpendicular to the z axis.

energy levels. The feasible operations are those occurring in the time scale of experimental conditions. Mulliken,[54] Hougen[55] and Longuet-Higgins[56] independently introduced the permutation-inversion group (also known as molecular symmetry group), which is the smallest subgroup of the direct product of complete permutation group of identical nuclei and space inversion group to compose of all feasible operations. It can be shown that for semi-rigid molecules, each feasible operation corresponds to a finite rotation of the whole molecule in space. In addition, their molecular symmetry group is isomorphic to the corresponding molecular point group based on geometric symmetry. On the other hand, permutation-inversion group assumes no geometry of the molecule so it can be used for systems without definite geometry, such as CH_5^+.

The application of group theory to matrix-isolated molecules was introduced by Miller and Decius based on the idea of feasibility in the theory of permutation-inversion group.[57] Unlike molecules in free space, matrix-isolated molecules are in an environment of finite symmetry. As a result, both molecular symmetry and crystal symmetry have to be considered in constructing the symmetry group. In the following, we will apply this theory to matrix-isolated diatomic molecules which are assumed to have nearly free rotation and vibration. Treatments of molecules not having rotation and vibration can be found in Ref. 57 and will not be discussed here.

The molecular symmetry group $\overline{M}$ of a heteronuclear diatomic molecule is composed of two operations:

$$\overline{M} = \{\overline{E}, \overline{E}^*\}, \tag{2-1}$$

where $\overline{E}$ and $\overline{E}^*$ are the identity and space inversion operation, respectively. We use overbar to distinguish the molecular symmetry operations as Miller and Decius. The point symmetry group of the *hcp* crystal is D_{3h}, which is composed of the following twelve operations:

$$D_{3h} = \{E, 2C_3, 3C_2, \sigma_h, 2S_3, 3\sigma_v\}, \tag{2-2}$$

where the C_3 axis is along the c axis of the crystal (i.e. Z axis) and the symbol of each operation is written in the standard point group notation.[58] The complete symmetry group of matrix-isolated AB is therefore the direct product of $\overline{M}$ and D_{3h}. It should be noted that an operation in D_{3h} with reflection converts the right-handed reference system to a left-handed one. This relative configuration between AB and the crystal cannot be obtained without breaking chemical bonds or crystal. In other words, they are not feasible operations at cryogenic temperature. The same argument applies to the operation $\overline{E}^*$ in the group of AB. As a result, both AB and the crystal have to undergo inversion/reflection *simultaneously* in order to maintain the same relative configuration as pointed out by Miller and Decius. Based on this consideration, the feasible symmetry operations for a rotational AB molecule in the D_{3h} crystal is composed of the following operations:

$$G_{12} = \{E, 2C_3, 3C_2\} \otimes \{\overline{E}\} + \{\sigma_h, 2S_3, 3\sigma_v\} \otimes \{\overline{E}^*\}, \tag{2-3}$$

Using the standard procedure in group theory, the operations in G_{12} can be derived as:

$$G_{12} = \{E\overline{E}, 2C_3\overline{E}, 3C_2\overline{E}, \sigma_h\overline{E}^*, 2S_3\overline{E}^*, 3\sigma_v\overline{E}^*\}, \tag{2-4}$$

The corresponding character table which can also be obtained using standard procedure is given in TABLE 2. Using this character table, one can easily classify the symmetry properties of rotational wavefunctions.

TABLE 2 Character table of group G_{12}.

G_{12}	$1E\overline{E}$	$2C_3\overline{E}$	$3C_2\overline{E}$	$1\sigma_h\overline{E}^*$	$2S_3\overline{E}^*$	$3\sigma_v\overline{E}^*$		
A_1'	1	1	1	1	1	1		$\alpha_{ZZ}, \alpha_{XX}+\alpha_{YY}$
A_2'	1	1	-1	1	1	-1		
E'	2	-1	0	2	-1	0	(μ_X, μ_Y)	$\alpha_{XY}, \alpha_{XX}-\alpha_{YY}$
A_1''	1	1	1	-1	-1	-1		
A_2''	1	1	-1	-1	-1	1	μ_Z	
E''	2	-1	0	-2	1	0		α_{XZ}, α_{YZ}

The rotational wavefunction $|J,M\rangle$ of a diatomic molecule is expressed in terms of spherical harmonics $C^*_{JM}(\theta,\phi)$ specified by the two polar angles (θ,ϕ),

$$|J,M\rangle = \sqrt{(2J+1)/8\pi^2}\, C^*_{JM}(\theta,\phi), \tag{2-5}$$

where J is the total angular momentum, M is the projection of J along the laboratory-fixed axis and polar angles (θ,ϕ) define the molecule-fixed axis system with respect to the crystal-fixed axis system. Here we follow the sign convention of Bunker and Jensen.[53]

The symmetry classification of the rotational wavefunctions under the extended group G_{12} can be obtained by considering the transformation properties of polar angles (θ,ϕ) and their effects on spherical harmonics. For example, the operation $C_3\overline{E}$ of extended group G_{12} can be interpreted as a C_3 rotation of the crystal together with an $\overline{E}$ operation of the AB molecule. Following the conversion of Miller and Decius, we fix the crystal in space and define $C_3\overline{E}$ to be a C_3^{-1} rotation of the molecule AB about crystal-fixed axes together with an $\overline{E}$ operation. Hence, the operation $C_3\overline{E}$ changes the polar angles (θ,ϕ) to $(\theta,\phi-2\pi/3)$. The transformation properties of polar angles (θ,ϕ) under the symmetry operations of group G_{12} are determined accordingly and listed in TABLE 3. Using the results, the transformation of the rotational wavefunction $|J,M\rangle$ follows

$$\begin{aligned}
&E\overline{E}|J,M\rangle = |J,M\rangle,\\
&C_3\overline{E}|J,M\rangle = e^{-2\pi i M/3}|J,M\rangle,\\
&C_2\overline{E}|J,M\rangle = (-1)^{J+M}|J,-M\rangle,\\
&\sigma_h\overline{E}^*|J,M\rangle = (-1)^{J-M}|J,M\rangle,
\end{aligned} \tag{2-6}$$

$$S_3\overline{E}^*\left|J,M\right\rangle = (-1)^J e^{\pi M/3}\left|J,M\right\rangle,$$
$$\sigma_v\overline{E}^*\left|J,M\right\rangle = \left|J,-M\right\rangle.$$

Using the relationships above, one can easily work out the irreducible representation of the rotational wavefunctions using the standard projection operator method. The results are shown in TABLE 4. From the table one can figure out the splitting pattern of each J manifold. For example, the $J = 1$ is split into $A_2"\oplus E'$ components while the $J = 2$ state is split into $A_1'\oplus E'\oplus E"$, respectively, in the D_{3h} crystal field.

In determining the symmetry of laboratory-fixed components of the dipole moment of AB, the same procedure is applied. For simplicity in the discussion later, we can consider the three spherical components instead of the Cartesian components. It is know that the three spherical components are first-ranked spherical tensor operators, which behave like spherical harmonics of $J = 1$. Applying the same argument as before, one has

$$\Gamma(\mu_Z) = A_2"; \tag{2-7}$$

$$\Gamma(\mu_X, \mu_Y) = E'. \tag{2-8}$$

2.2. Crystal Field Splitting

After the qualitative analysis of the symmetry of an AB molecule isolated in the *hcp* crystal field, we will discuss quantitatively the crystal field splitting of its rovibrational levels. As we discussed before, the guest molecule AB is assumed to vibrate and rotate freely in the crystal field. Due to the anisotropic crystal environment, different orientations of AB molecule with respect to the crystal-fixed

TABLE 3 Values of the polar angles (θ,ϕ) corresponding to the symmetry operations of group G_{12}.

Operation	θ	ϕ
$E\overline{E}$	θ	ϕ
$C_3\overline{E}$	θ	$\phi-\frac{2\pi}{3}$
$C_2\overline{E}$	$\pi-\theta$	$-\phi$
$\sigma_h\overline{E}^*$	$\pi-\theta$	ϕ
$S_3\overline{E}^*$	$\pi-\theta$	$\phi+\frac{4\pi}{3}$
$\sigma_v\overline{E}^*$	θ	$-\phi$

TABLE 4 Symmetry classification of the rotational wavefunctions of G_{12}.

Rotational quantum number	J even	J odd
$\lvert M\rvert = 0 (\mathrm{mod}\, 6)$	A_1'	A_2''
$\lvert M\rvert = 1 (\mathrm{mod}\, 6)$	E''	E'
$\lvert M\rvert = 2 (\mathrm{mod}\, 6)$	E'	E''
$\lvert M\rvert = 3 (\mathrm{mod}\, 6)$	$A_1'' \oplus A_2''$	$A_1' \oplus A_2'$
$\lvert M\rvert = 4 (\mathrm{mod}\, 6)$	E'	E''
$\lvert M\rvert = 5 (\mathrm{mod}\, 6)$	E''	E'

axis will have different energies. As a result, the M sublevels in each J manifold of the AB molecule, while degenerate in free space, are now split according to the crystal symmetry. Since there is no significant overlap in electron clouds between the guest molecule and the host crystal, the only interaction to be considered is the long-range electrostatic interaction. Assuming the impurity molecules are far separated so that their interactions can be neglected, we only need to consider the interactions between the host crystal and the impurity molecules. For parahydrogen at cryogenic temperature, there is no permanent dipole and higher order multipoles due to the spherically symmetric rotational wavefunction. However, the permanent dipole and quadrupole of the impurity molecule AB can induce a dipole on the surrounding p-H_2 molecules. According to electrostatic theory, the electric field at a position $\boldsymbol{R}_\rho$ from the central impurity molecule produced by its multipole of order l has the form[24]

$$E_m^l(R_\rho) = (-1)^m \sqrt{(l+1)(2l+1)} \sum_v Q_l C_{lv}(\Omega) C(1,l,l+1;m\bar{v}) \frac{C^*_{l+1,v-m}(\Omega_\rho)}{R_\rho^{l+2}}, \qquad (2\text{-}9)$$

where $C(1,l,l+1;m\bar{v})$ are Clebsch-Gordan coefficients, $C_{lv}(\Omega)$ and $C^*_{l+1,v-m}(\Omega_\rho)$ are Racah spherical harmonics describing the orientation of the central molecule (Ω) and the vector $\boldsymbol{R}_\rho$, respectively, and $Q_l \equiv \langle vJ|Q_l(r)|vJ\rangle$ is the permanent multipole moment of order l of the central molecule. For a p-H_2 molecule located at R_ρ with isotropic polarizability α and anisotropic polarizability γ, the induced dipole moment has the form[24]

$$\mu_m(R_\rho) = \alpha(r)E_m(R_\rho) - \frac{\sqrt{10}}{3}\gamma(r)\sum_\mu C(211;\mu,m-\mu)C_{2\mu}(\Omega_\rho)E_{m-\mu}(R_\rho), \quad (2\text{-}10)$$

where $\alpha(r)$ and $\gamma(r)$ are the isotropic and anisotropic parts of the polarizability for the given internuclear separation $\boldsymbol{r}$. This induced dipole moment will interact with the original multipole moment of the central molecule to produce an extra binding energy

$$\varepsilon_l = -\alpha \sum_m (-1)^m E_m(R_\rho) E_{\bar{m}}(R_\rho) + \frac{\sqrt{10}}{3} \gamma \sum_m (-1)^m \sum_\mu C(211;\mu, m-\mu) C_{2\mu}(\Omega_\rho) E_{m-\mu}(R_\rho) E_{\bar{m}}(R_\rho), \tag{2-11}$$

where $\alpha \equiv \langle 00|\alpha(r)|00\rangle$ and $\gamma \equiv \langle 00|\gamma(r)|00\rangle$ are the isotropic and anisotropic polarizability of the p-H_2 molecules, respectively. The anisotropic effect of the extra binding energy is zero due to vanishing matrix element of $C_{2\mu}(\Omega_\rho)$ for p-H_2 molecules in $J = 0$ state. The isotropic effect is then summed over for all surrounding p-H_2 molecules to give

$$\xi_l^{pol} = -\frac{1}{2} \alpha \sum_\rho{}' \sum_m (-1)^m E_m(R_\rho) E_{\bar{m}}(R_\rho). \tag{2-12}$$

For $l = 1$, we have dipole induced dipole interaction, whose energy correction is

$$\xi_1^{pol} = 15 \frac{\alpha Q_1^2}{R_0^6} \sum_{l=0,2} \begin{Bmatrix} 2 & 2 & l \\ 1 & 1 & 1 \end{Bmatrix} C(11l;000) C(22l;000) \times \sum_m (-1)^m C_{lm}(\Omega) \sum_\rho{}' \left(\frac{R_0}{R_\rho}\right)^6 C_{l\bar{m}}(\Omega_\rho); \tag{2-13}$$

For $l = 2$, we have quadrupole induced dipole interaction, whose energy correction is

$$\xi_2^{pol} = \frac{105}{2} \frac{\alpha Q_2^2}{R_0^8} \sum_{l=0,2,4} \begin{Bmatrix} 3 & 3 & l \\ 2 & 2 & 1 \end{Bmatrix} C(22l;000) C(33l;000) \times \sum_m (-1)^m C_{lm}(\Omega) \sum_\rho{}' \left(\frac{R_0}{R_\rho}\right)^8 C_{l\bar{m}}(\Omega_\rho). \tag{2-14}$$

The correction energy, which is proportional to $R_\rho^{-2(l+2)}$, drops off rapidly with increasing l. We therefore stop the consideration at $l = 2$.

After evaluating the corresponding *6-j* symbol and the lattice sum, one can obtain general expressions:

$$\xi_1^{pol} = \varepsilon_{2c} C_{20}(\Omega) \tag{2-15}$$

for the dipole-induced dipole effect,

and

$$\xi_2^{pol} = \varepsilon_{2c} C_{20}(\Omega) + \varepsilon_{4c} C_{40}(\Omega) \tag{2-16}$$

for the quadrupole-induced dipole effect, respectively.

The determination of the crystal field parameters ε_{2c} and ε_{4c} requires the knowledge of the lattice sum, matrix element $\langle 00|\alpha(r)|00\rangle$ of *p*-H_2, and matrix element $\langle vJ|Q_l(r)|vJ\rangle$ of the central molecule. In the following section, the evaluation of $\langle vJ|Q_l(r)|vJ\rangle$ will be discussed.

2.3. Permanent Multipole Moment

From the discussion in Section 2.2, the total polarization energy depends on the matrix elements of molecular multipole moment $\langle vJ|Q_l(r)|vJ\rangle$. In the following, the numerical determination of this matrix element under the adiabatic approximation will be outlined. [59]

Due to the axial symmetry of a diatomic molecule, the strength of 2^l-pole moment tensor of rank l is characterized by a single component Q_l along the molecular axis. The static multipole moment along the molecular axis is expressed as the sum of two terms, independently representing the contributions from the nuclei and electrons[24]

$$Q_l(r) = e\left[2Z(r/2)^l - \sum_{el}\left\langle r_{el}^l P_l(\cos\theta)\right\rangle\right], \tag{2-17}$$

where e is the electronic charge, Z is the atomic number of the nuclei, r is intermolecular distance and θ is the polar coordinate of the electron. The summation is for all electrons and expectation value is for the electronic wavefunctions $\psi(r_{el}, r)$ in the adiabatic approximation relevant to the clamped nuclear problem.[24] The adiabatic values for the radial matrix elements of the multipole moments are the defined by

$$\left\langle vJ\left|Q_l(r)\right|v'J'\right\rangle = \int_0^\infty u_{vJ}(r)Q_l(r)u_{v'J'}(r)dr\,, \tag{2-18}$$

where u_{vJ} denotes the radial part of the rotation-vibrational wavefunction. Under the adiabatic approximation, the nuclear and electronic motions are decoupled. The rotation-vibration energy levels and the corresponding radial wavefunctions u_{vJ} can be found by solving the nuclear Schrödinger equation of a diatomic molecule:[60]

$$\hat{H}u_{vJ}(r) = E_{vJ}u_{vJ}(r)\,, \tag{2-19}$$

where $$\hat{H} = -\frac{\hbar^2}{2\mu}\frac{d^2}{dr^2} + U_0(r) + \frac{J(J+1)\hbar^2}{2\mu r^2}\,,$$

$\mu = m_1 m_2 / m_1 + m_2$ is the reduced mass of the two nuclei, $U_0(r)$ is the vibrational potential depending on the radial distance r of the two nuclei, and v and J denote the vibrational and rotational quantum numbers, respectively. The last term in $\hat{H}$ accounts for the centrifugal potential energy due to molecular rotation. It should be pointed out that this equation does not assume any separation between rotational and vibrational motions. It remains valid as far as the adiabatic approximation holds.

Once the potential $U_0(r)$ of the molecule is known, the wavefunctions $u_{v,J}$ can be obtained by solving the one-dimensional Schrödinger equation (2-19) for $r > 0$ with an effective potential energy equal to the sum of $U_0(r)$ and the term $\frac{J(J+1)\hbar^2}{2\mu r^2}$. To solve Eq. (2-19), one assumes that the radial wavefunctions $u_{v,J}$ can be expanded by a complete set of basis functions $\chi_n(\xi)$:

$$u_{v,J}(r) = \sum_n c_n \chi_n(\xi), \tag{2-20}$$

where $$\chi_n(\xi) = \left(\frac{\alpha}{\sqrt{\pi}\, 2^n n!}\right)^{1/2} \bullet \exp\left(-\alpha^2 \xi^2 / 2\right) H_n(\alpha\xi)$$

is the normalized eigenfunction of simple harmonic oscillator with expansion coefficient C_n, $H_n(\alpha\xi)$ is Hermite polynomial, ξ is the displacement from equilibrium position r and the equilibrium distance r_e (i.e. $\xi = r - r_e$), and α is a parameter for the molecule which has the value $\alpha = \sqrt{\mu\omega_0 / \hbar}$.

Since the expansion coefficients c_n satisfy the set of equations

$$\sum_n (\hat{H}_{mn} - E_{v,J}\delta_{mn}) c_n = 0, \tag{2-21}$$

with $$\hat{H}_{mn} = \int \chi_m^* \hat{H} \chi_n d\xi .$$

The eigenvalues $E_{v,J}$ and eigenvectors $u_{v,J}$ can be obtained by solving secular equation

$$\det(\hat{H}_{mn} - E\delta_{mn}) = 0 . \tag{2-22}$$

Using the solutions of Eq. (2-22), the adiabatic values for the radial matrix elements of the multipole moments $Q_l(r)$ can be computed using Eq. (2-18).

2.4. Predicted Rovibrational Spectrum

In predicting the rovibrational spectrum of matrix-isolated molecules, we need to determine the transition dipole moment among different rovibrational states. Since the dipole operator can be expressed by the components with respect to two different Cartesian axis systems, one fixed in the laboratory, the other rotating with the molecule. In considering the dipole interaction between the photon field and the matrix-isolated molecule, the dipole operator referred to the laboratory–fixed axes (μ_X, μ_Y, μ_Z) should be used. On the other hand, the symmetry of the molecules allows us to determine the nonzero components of dipole referred to the molecule-fixed components (μ_x, μ_y, μ_z) easily. These two set of components are related by either the Euler angles (χ, θ, ϕ) for nonlinear molecules or the polar angles (θ, ϕ) for diatomic and linear molecules. For a diatomic molecule in the D_{3h} crystal field, only μ_z in molecule-fixed axis system is nonzero. Therefore, the laboratory–fixed Cartesian components of the dipole operator can be expressed as

$$\begin{aligned} \mu_Z &= \mu_z \cos\theta ; \\ \mu_X &= \mu_z \sin\theta \cos\phi ; \\ \mu_Y &= \mu_z \sin\theta \sin\phi . \end{aligned} \tag{2-23}$$

These components can be written in the form of spherical tensor operators:[24]

$$\begin{aligned} \mu_0 &= \mu_Z = \cos\theta \bullet \mu_z = C_{10} \bullet \mu_z , \\ \mu_{\pm 1} &= \frac{1}{\sqrt{2}}(\mu_X \pm i\mu_Y) = \frac{1}{\sqrt{2}} e^{\pm i\phi} \sin\theta \bullet \mu_z = C_{11} \bullet \mu_z , \end{aligned} \tag{2-24}$$

where μ_0 gives the dipole moment component parallel to the crystal c axis, while $\mu_{\pm 1}$ give the dipole moment components perpendicular to the crystal c axis.

The absorption intensity (I) of a spectral transition is proportional to population in the initial state and the square of the corresponding transition dipole moment, i.e.

$$I \propto N_i \left|\langle v'|\mu_z|v\rangle\right|^2 \left|\langle J'M'|C_{1m}|JM\rangle\right|^2, \tag{2-25}$$

where $N_i = g_i e^{-E_i/k_B T}$,

N_i is the equilibrium population of molecules in the initial state with eigenvalue E_i. The vibrational dependence of the transition dipole moment $\langle v'|\mu_z|v\rangle$ can be dropped out in the calculation of relative intensity since it is the same for all transitions in the same vibrational band. For the transitions due to light with polarization parallel to the crystal c axis, the operator μ_0 is used. On the other hand, $\mu_{\pm 1}$ should be used for light with polarization perpendicular to the crystal c axis. It is noted that the value $\langle v'|\mu_z|v\rangle$ cannot be zero in order to have the allowed vibrational transition. Therefore, the vibrational selection rule $\Delta v = \pm 1$ is required. Similarly, the rotational selection rule $\Delta J = \pm 1$ resulted from the parity requirement also applies to the system. From Eq. (2-25), it is seen that the matrix element $\left|\langle J'M'|C_{1m}|JM\rangle\right|$ is nonzero only when $M' = m + M$. This gives rise to the $\Delta M = 0, \pm 1$ selection rules corresponding to parallel and perpendicular polarization, respectively. Combining the results in Section 2.1, one can easily determine the relative intensities of the allowed transitions.

CHAPTER 3

APPLICATION: CARBON MONOXIDE IN SOLID PARAHYDROGEN

The theoretical model established in Chapter 2 has been applied to the case of CO embedded in parahydrogen. In this chapter, the results will be presented. The radius of CO is about 1.62Å, which is distinctly smaller than the intermolecular distance of 3.793Å of solid parahydrogen.[42] It is expected that CO occupying a lattice site will not introduce severe distortion to the crystal. Due to the weak intermolecular interactions in parahydrogen crystal, we also assumed that CO impurity molecules vibrate and rotate in the crystal field with little hindrance. The M splitting, multipole moment, and relative intensities of the transitions in the fundamental band of CO were computed using our theoretical framework.

3.1. Permanent Multipole Moment of CO

In order to determine the crystal field splitting of rovibrational energy levels, the multipole moment of CO was calculated following the prescription in Section 2.3. To determine the matrix elements $\langle vJ|Q_l|v'J'\rangle$, the knowledge of vibrational wavefunction is required. In solving Eq. (2-19) to obtain the modified rotation-

vibration wavefunction u_{vJ} numerically, the Hulbert-Hirschfelder (*H-H*) potential function[61] which gave the best average results when compared to the available Rydberg-Klein-Rees (*RKR*) data[62] was used to expressed $U_0(r)$, i.e.

$$U_0(r) = D[(1-e^{-x})^2 + cx^3 e^{-2x}(1+bx)]$$

$$\text{with} \qquad x = \frac{\omega_e}{2\sqrt{B_e D}}\left[\frac{r-r_e}{r_e}\right], \tag{3-1}$$

where r_e, ω_e, B_e are spectroscopic constants given by Herzberg,[42] and the parameters D, c, b are determined from these spectroscopic constants according to Ref. 61. All the values of these constants/parameters are given in Ref. 61 and reproduced in TABLE 5.

Using the lowest 15 harmonic oscillator wavefunctions as basis functions, u_{vJ} were obtained by solving the secular equations. In TABLE 6, the expansion coefficients of the lowest four u_{vJ} states are listed.

In determining the dipole moment matrix, we adopted the approach by Kirschner *et al.* based on the Padé approximant to express the dipole function by[63]

$$Q_1(x) = \frac{M_0(1 + C_1 x + C_2 x^2)}{1 + C_3 x + C_4 x^2 + C_5 x^3 + C_\infty x^6} \tag{3-2}$$

$$\text{with} \qquad x = (r - r_e)/r_e .$$

TABLE 7 shows the parameters M_0, C_1, C_2, C_3, C_4, C_5, and C_∞ for CO listed in Ref. 64, which were obtained by fitting the Padé approximant expression Eq. (3-2) to the rigorous expression Eq. (2-17). Based on Eq (3-2), the matrix elements $\langle vJ|Q_1(r)|v'J'\rangle$ were then calculated using the wavefunctions u_{vJ} and $u_{v'J'}$.

TABLE 5 Parameters for *H-H* potential curve of CO molecule. [61]

Parameter	Value
$\omega_e(cm^{-1})$	2168.2
$B_e(cm^{-1})$	1.9310
$\alpha_e(cm^{-1})$	0.01744
$r_e(\mathring{A})$	1.1284
$D(cm^{-1})$	74.840
c	0.0567
b	1.568

TABLE 6 The expansion coefficients of the lowest four $u_{v,J}$ states. (Numbers in parentheses refer to powers of ten)

	u_1	u_2	u_3	u_4
c_1	9.98040(-01)	-6.02884(-02)	-1.87125(-03)	1.49001(-02)
c_2	6.01996(-02)	9.83017(-01)	1.68872(-01)	-1.65776(-02)
c_3	3.40207(-03)	1.68276(-01)	-9.35116(-01)	3.01138(-01)
c_4	1.65814(-02)	2.04820(-02)	-2.99101(-01)	-8.35065(-01)
c_5	2.22832(-03)	3.47615(-02)	-5.76572(-02)	-4.30947(-01)
c_6	2.16157(-04)	9.54560(-03)	-5.97659(-02)	-1.17835(-01)
c_7	6.19919(-04)	1.74284(-03)	-2.46877(-02)	-9.42888(-02)
c_8	1.20549(-04)	1.84686(-03)	-6.61101(-03)	-5.03532(-02)
c_9	1.58852(-05)	6.41442(-04)	-4.54290(-03)	-1.78397(-02)
c_{10}	3.18827(-05)	1.48420(-04)	-2.10052(-03)	-1.02464(-02)
c_{11}	7.96572(-06)	1.22701(-04)	-6.76708(-04)	-5.46213(-03)
c_{12}	1.30245(-06)	4.92524(-05)	-3.94044(-04)	-2.19916(-03)
c_{13}	1.99031(-06)	1.33380(-05)	-1.91188(-04)	-1.13186(-03)
c_{14}	5.91597(-07)	9.09116(-06)	-6.60488(-05)	-5.71762(-04)
c_{15}	6.36168(-08)	3.31315(-06)	-2.97472(-05)	-1.88827(-04)

TABLE 7 Parameters in least-squares fits to $Q_1(r)$. [64]

Parameter	Value
M_0	-0.126 a.u.
C_1	10.0958
C_2	5.2609
C_3	0.5512
C_4	1.1407
C_5	0.3827
C_∞	0.2057

Since we are interested in the first few vibrational states, which have very small amplitude at the large internuclear separation, the integration limit was set between 1 to 3 a_0 for simplicity. TABLE 8 shows the diagonal matrix elements for the first two vibrational levels.

The approximate quadrupole moment function proposed by Truhlar[65]

$$Q_2(r) = \sum_{i=0}^{n} Q_i (r - r_e)^i \tag{3-3}$$

was used to determined the quadrupole moment matrix. TABLE 9 lists the parameters Q_i in Eq. (3-3) for CO molecules.[66,67] This approximate expression works for small vibrational amplitude (i.e. r not far from r_e), which is the case for the first few vibrational states. Using this function and wavefunctions u_{vJ} and $u_{v'J'}$, the matrix elements of quadrupole moment $\langle vJ|Q_2(r)|v'J'\rangle$ were obtained. Once again, , the integration limit was set between 1 to 3 a_0. The results of this calculation are shown in TABLE 10.

3.2. Crystal field splitting

With the multipole moment matrix determined, the crystal field splitting in each J manifold can be calculated. Since the dipole moment of CO is very small (~ 0.05 a.u.),[68] its effect on the crystal field splitting is much smaller compared to the quadrupole effect:

$$\frac{\alpha Q_1^2}{R_0^6} : \frac{\alpha Q_2^2}{R_0^8} \sim 0.1 \text{ cm}^{-1} : 1.3 \text{ cm}^{-1}$$

TABLE 8 Adiabatic matrix elements of the dipole moment for CO, in a.u.

v	J	$\langle vJ\|Q_1(r)\|vJ\rangle$
0	0	-0.12102
0	1	-0.12101
0	2	-0.12099
0	3	-0.12097
0	4	-0.12094
1	0	-0.11206
1	1	-0.11205
1	2	-0.11203
1	3	-0.11201
1	4	-0.11198
2	0	-0.10305
3	0	-0.09397
4	0	-0.08486

TABLE 9 Parameters in least-squares fits to $Q_2(r)$. [66,67]

Parameter	Value (*a.u.*)
n	2
Q_0	-2.6489
Q_1	1.2758
Q_2	0.45203

TABLE 10 Adiabatic matrix elements of the quadrupole moment for CO, in a.u.

v	J	$\langle vJ\|Q_2(r)\|vJ\rangle$
0	0	-2.63624
0	1	-2.63622
0	2	-2.63619
0	3	-2.63613
0	4	-2.63606
1	0	-2.61245
1	1	-2.61243
1	2	-2.6124
1	3	-2.61234
1	4	-2.61227
2	0	-2.58806
3	0	-2.56304
4	0	-2.53739

Using the Eq. (2-13) and Eq. (2-14) in Section 2.2 and the values of the constants (α = 5.41 *a.u.*, R_0 = 3.793Å), we can calculate the total polarization energy by performing a lattice sum. The detail distances and numbers of neighbors of *hcp* crystal of each shell are listed in TABLE 11.[69] Due to the high power dependence of R_p, the effect will drop off very fast as R_p increases. We have therefore taken into account twenty nearest shells of neighbors in summing the *hcp* lattice effect. It was found that in the case of dipole-induced dipole effect, the crystal symmetry gives rise to almost complete cancellation in the lattice sum. As a result, its overall effect on the crystal field splitting is negligible.

On the other hand, the effect quadrupole-induced dipole interaction on the M splitting was calculated according to Eqs. (2-14), (2-16), and the matrix elements obtained in the previous section. The difference of the total polarization energy between the $v = 0$ and $v = 1$ states arise from the different quadrupole moment matrix of CO in the $v = 0$ and $v = 1$ states.

The crystal field splitting of the rovibrational states of CO in p-H_2 was then calculated from the matrix elements $\langle JM|C_{20}|JM\rangle$ and $\langle JM|C_{40}|JM\rangle$ which are listed in TABLE 12 for the first few J manifolds. The energy splitting and shifts of these levels were calculated by combining the results in TABLE 10, 11, and 12 and shown in TABLE 13. Since the pure vibrational frequency is not known accurately but a constant for all transitions, we take it as our zero energy point. The corresponding splitting pattern is also shown in FIG 4.

TABLE 11 The distances and numbers of neighbors in successive shells in the *hcp* crystal.

i	$(R_i/R_0)^2$	n_i	i	$(R_i/R_0)^2$	n_i
1	1	12	11	20/3	12
2	2	6	12	7	24
3	8/3	2	13	22/3	6
4	3	18	14	25/3	12
5	11/3	12	15	9	12
6	4	6	16	29/3	24
7	5	12	17	10	12
8	17/3	12	18	31/3	12
9	6	6	19	32/3	2
10	19/3	6	20	11	12

TABLE 12 The matrix elements $\langle JM|C_{20}|JM\rangle$ and $\langle JM|C_{40}|JM\rangle$ for the first few J manifolds.

J	$\|M\|$	$\langle JM\|C_{20}\|JM\rangle$	$\langle JM\|C_{40}\|JM\rangle$
0	0	0	0
1	0	$\frac{2}{5}$	0
1	1	$-\frac{1}{5}$	0
2	0	$\frac{2}{7}$	$\frac{2}{7}$
2	1	$\frac{1}{7}$	$-\frac{4}{21}$
2	2	$-\frac{2}{7}$	$\frac{1}{21}$

TABLE 13 Calculated energy levels and shifts of the ground state and excited state of CO molecule.

	Energy (cm^{-1})		Symmetry	Energy shifts (cm^{-1})
Ground state				
$J=0$	0	$\|M\|=0$	A_1'	0.000
$J=1$	3.845	$\|M\|=0$	A_2''	-0.001628
		$\|M\|=1$	E'	0.0008140
$J=2$	11.53	$\|M\|=0$	A_1'	-0.5081
		$\|M\|=1$	E''	0.3374
		$\|M\|=2$	E'	-0.08333
Excited state				
$J=0$	0	$\|M\|=0$	A_1'	0.000
$J=1$	3.810	$\|M\|=0$	A_2''	-0.001600
		$\|M\|=1$	E'	0.0007999
$J=2$	11.43	$\|M\|=0$	A_1'	-0.4990
		$\|M\|=1$	E''	0.3313
		$\|M\|=2$	E'	-0.08183

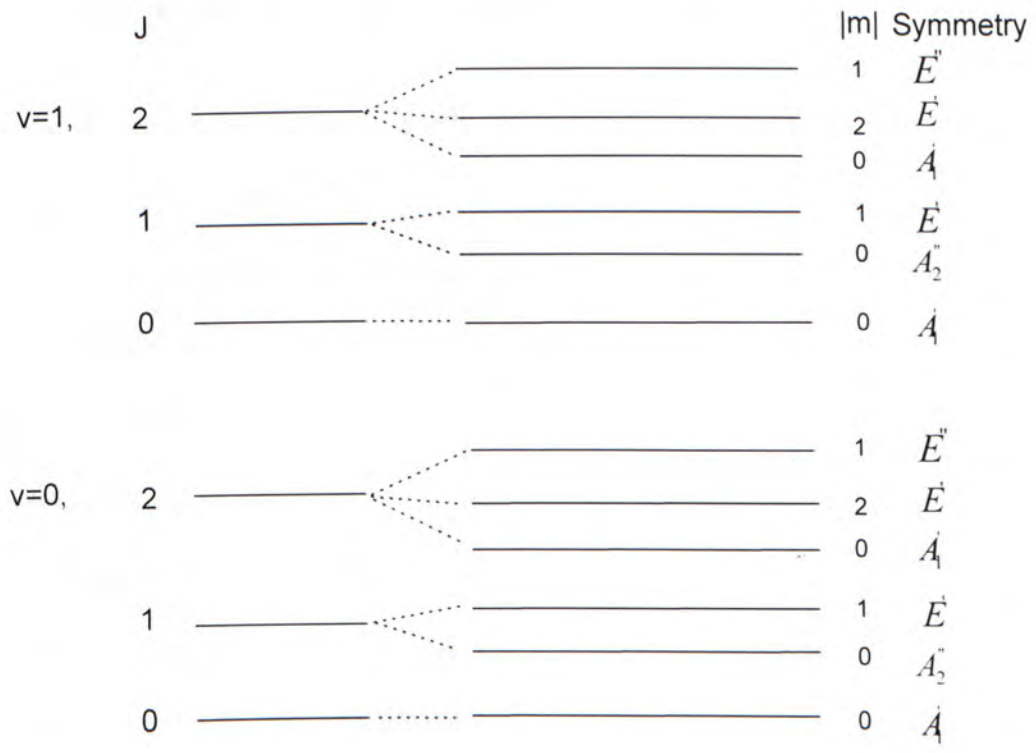

FIGURE 4 Rovibratinal energy level diagrams of CO in p-H_2. The energy levels at the left-hand side are those without the crystal field while those at the right-hand side are with the crystal.

3.3. Rovibrational Transitions and Relative Intensities

At a temperature of ~ 4.2 K, the population ratio for the first few J manifolds was about $1(J=0)$: $0.8(J=1)$: $0.1(J=2)$: $0.002(J=3)$ according to Boltzmann distribution. In calculating the relative intensities, we only considered levels to $J=2$. Based on the results of group theory discussed in Section 2.1, the allowed transitions due to parallel and perpendicular polarizations are shown in FIG. 5. It is seen that these transitions also satisfy the selection rules for angular momentum $\Delta J = \pm 1$ and $\Delta v = \pm 1$ suggesting the consistency of different approaches.

The relative intensities of the allowed transitions in the $v = 1 \leftarrow 0$ band are calculated based on the Eq. (2-25). The results are shown in TABLE 14. In the table the transition frequencies, polarization dependence, and the relative intensities are also shown. Once again, the zero point frequency point corresponds to the transitions frequency of the $v = 1 \leftarrow 0$ transition.

Based on the relative intensities, a computer-generated spectrum diagram is shown in FIG. 6 to predict the observable rovibational band. The Guassian line profiles are also shown for the transitions using a linewidth of $\sim 0.1 \text{cm}^{-1}$ (HWHM). While 14 transitions are predicted in groups of R(0), R(1), P(1), and P(2), respectively, the broad width of CO may smear out most of the fine structure and gives rise to only four transitions.

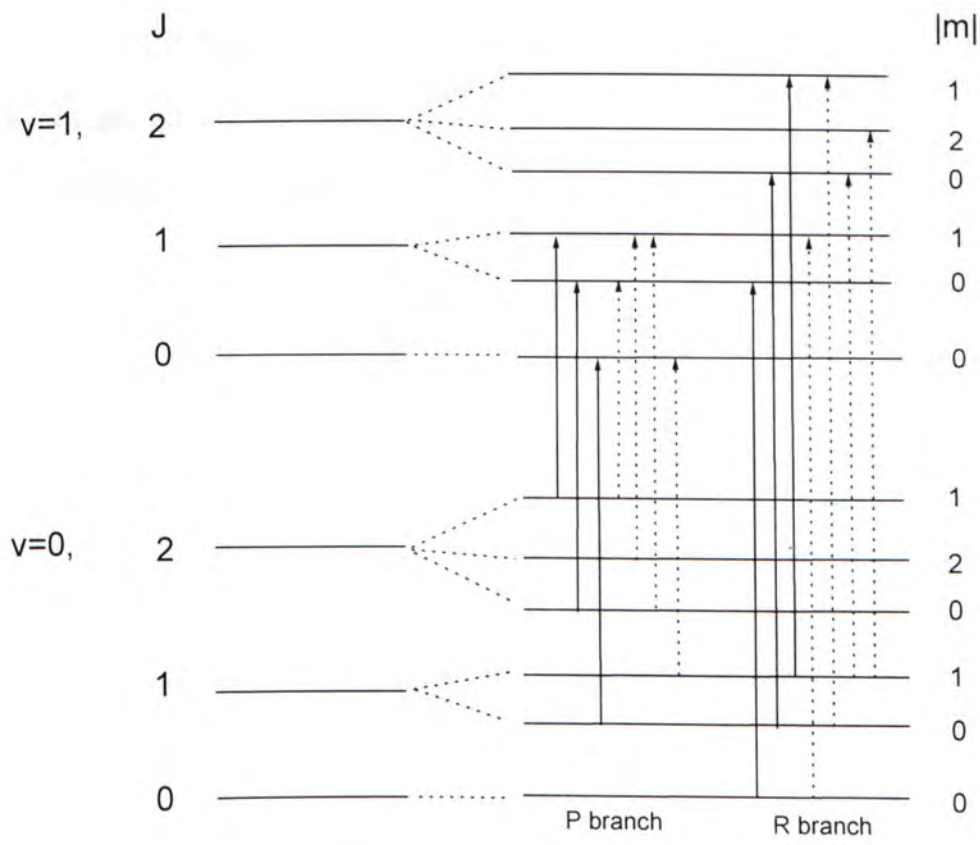

FIGURE 5 The *J=0~2* rovibrational levels of the ground vibrational state and excited vibrational state with the transitions among these levels. The vertical solid arrows indicate the allowed transitions for light polarized parallel to the *c* axis and the doted perpendicular to the *c* axis. The left-hand side transitions are P transitions and the right-hand side transitions are R transitions.

TABLE 14 Differences between the calculated level energies for CO in p-H_2, the frequencies shown are calculated from $\Delta E(v=1,J'M') - \Delta E(v=1,J'M')$

No.	polarization dependence	$v = 1$ $J'\ M'$	$v = 0$ $J\ M$	Calculated Freq. (cm^{-1})	calculated Intensity
1	z	0 0	1 0	-3.843	0.089
2	±	0 0	1 1	-3.846	0.089
3	z	1 0	2 0	-7.218	0.022
4	z	1 1	2 1	-8.062	0.013
5	±	1 0	2 1	-8.064	0.013
6	±	1 1	2 2	-7.641	0.029
7	±	1 1	2 0	-7.216	0.0056
8	z	1 0	0 0	3.808	0.090
9	±	1 1	0 0	3.811	0.090
10	z	2 0	1 0	7.088	0.024
11	z	2 1	1 1	7.915	0.013
12	±	2 1	1 0	7.918	0.013
13	±	2 2	1 1	7.502	0.031
14	±	2 0	1 1	7.085	0.0059

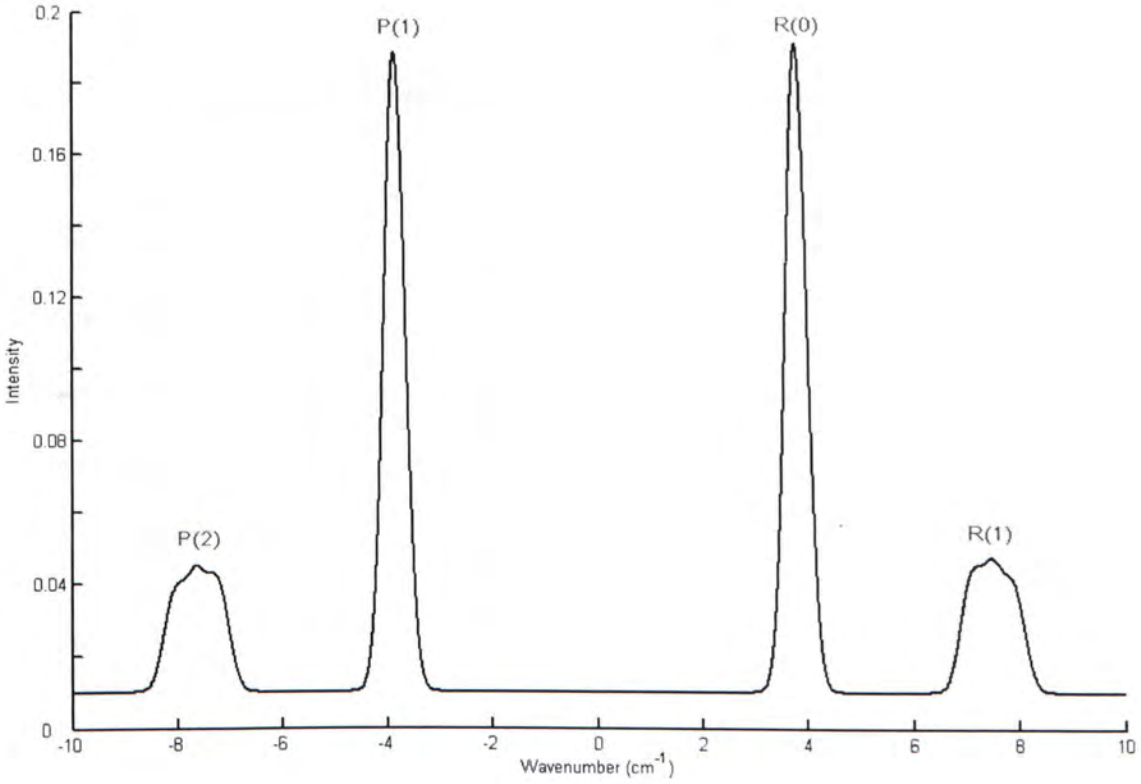

FIGURE 6 Predicted rovibrational spectrum of CO molecule. The spectral linewidth of 0.1 cm^{-1} (HWHM) was assumed. The symmetry center of wavenumber ($0cm^{-1}$) is the vibration transition between $v = 0$ and $v = 1$ states. The left-hand side spectral lines are from P transitions and the right-hand side spectral lines are from R transitions.

CHAPTER 4

DISCUSSION AND CONCLUSION

In this thesis, the theoretical model to study the crystal field splitting of heteronuclear diatomic molecules trapped in a *hcp* parahydrogen crystal has been established from the first principles. This approach, although developed for parahydrogen crystal, can be used for other systems with only slight modification. While a number of approximations have been made in our scheme, the result is expected to be at least semi-quantitatively consistent with the observation. An important correction yet to be considered is the phonon renormalization effect arising from the phonon averaging of the intermolecular separation R_0 in the lattice sum. Due to the large zero point lattice vibration of p-H_2 (~20% of R_0) in the crystal, this effect can be as great as 10%. While there are models to estimate its effects, reliable prediction in global cases has yet to be made.[20,70,71] The anisotropic dispersion effect is not considered in this calculation. Due to the symmetry of the system, it will have the same angular dependence as the induction effect. In other words, it will not be distinguished experimentally from the induction effect. The evaluation of its importance requires the knowledge of intermoleacular potential between CO and p-H_2.

A preliminary Fourier-Transform Infrared (*FTIR*) study of CO molecule embedded in solid p-H_2 at 4.2 K is shown in FIG. 7. This spectrum was recorded under the following experimental conditions: the parahydrogen crystal contains about 0.06 % orthohydrogen and mixes with ~ 7 ppm of CO. The optical length of the cell

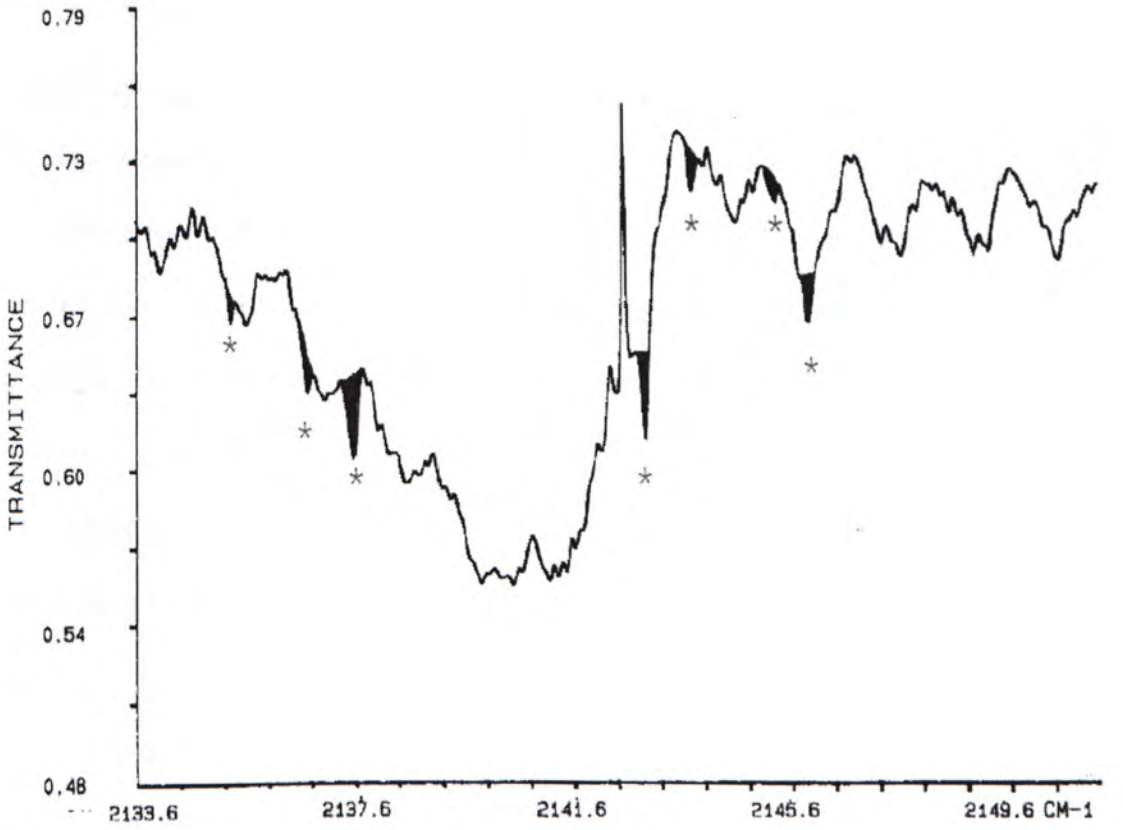

FIGURE 7 FTIR spectrum of CO isolated in solid parahydrogen.

is 0.7 cm. Seven transitions marked with asterisks were clearly seen in the spectrum. Based on our calculations, four of them fit to the pattern obtained in our calculations with good agreement in frequencies and relative intensity shown in FIG. 8. From the observed spectrum, the vibrational frequency was estimated to be about 2140cm^{-1}, slightly lower than the gas phase value.[72] This is expected from the weak solid state interactions in p-H_2 crystal. For a more definite assignment, the polarization dependence of the transitions should be studied using the polarized high resolution laser radiation. While the assignments only semi-quantitatively fit our model, we have little doubt that our theoretical study will provide some insight to study the high resolution rovibrational spectra of the heteronuclear diatomic molecules isolated in a D_{3h} solid parahydrogen field.

The nature of the other three unassigned transitions has yet to be explored. These lines have nearly equal intensities and linewidths as those assigned lines. It is found that each line has a neighboring transition separated by almost exactly ~ 0.7 cm^{-1} which is unlikely to be accidental. To date, we have not made any definite assignment but the idea of working along the line of perturbations of CO by a nearest neighboring o-H_2 molecule is being formulated.

The observed spectrum of CO indicates that it can rotate and vibrate in p-H_2 crystal. However, the M splitting of rotational energy levels has not been revealed due to the broad linewidth. The line broadening mechanism in this system is worth studying in order to understand the spectrum.

In conclusion, a semi-quantitative theory to study the rovibrational crystal field splitting of matrix isolated diatomic molecules has been established from the first

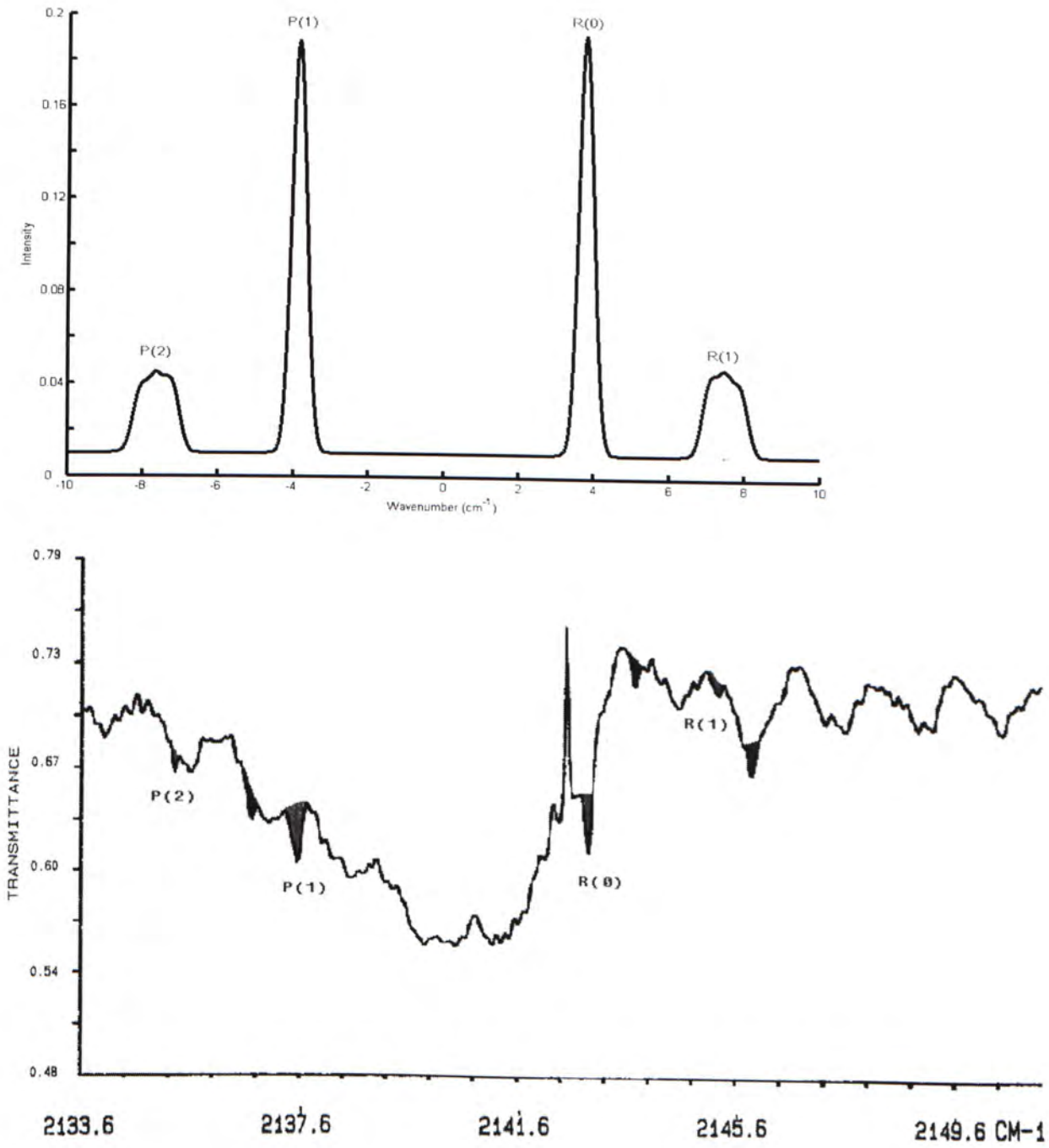

FIGURE 8 The assignment of FTIR spectrum of CO molecule in solid parahydrogen based on the comparison of (a) observed spectrum and (b) the theoretical spectrum.

principles. This theory was applied to the case of CO in solid p-H_2. Attempts at making spectral assignments based on the prediction were made. While the preliminary results are promising, some observed features in the spectrum are yet to be assigned suggesting that more theoretical studies are needed.

REFERENCE

1. Martin A. van der Hoef, , *J. Chem. Phys.*, **113**, 18 (2000)
2. T. G. Metzger, D. M. Gerguson, and W. A. Glauser, *J. Comput. Chem.* **18**, 70 (1997).
3. R. L. Rowley and T. Pakkanen, *J. Chem. Phys.*, **110**, 7 (1999)
4. M. Waldman and A. T. Hagler, *J. Comput. Chem.* **14**, 1077 (1993).
5. H. P. Gush, W. F. J. Hare, E. J. Allin, and H. L. Welsh, *Can. J. Phys.* **38**, 176 (1960).
6. S. S. Bhatnagar, E. J. Allin, and H. L. Welsh, *Can. J. Phys.* **57**, 933 (1962).
7. W. N. Hardy and A. J. Berlinsky, *Phys. Rev. Lett.* **34**, 1520 (1975).
8. W. N. Hardy, A. J. Berlinsky, and A. B. Harris, *Can. J. Phys.* **55**, 1150 (1977).
9. A. B. Harris, A. J. Berlinsky, and W. N. Hardy, *Can. J. Phys.* **55**, 1180 (1977).
10. B. W. Statt, W. N. Hardy, and R. Jochemsen, *Can. J. Phys.* **58**, 1326 (1980).
11. B. W. Statt and W. N. Hardy, *Can. J. Phys.* **58**, 1341 (1980).
12. R. Jochemsen, B. W. Statt, and W. N. Hardy, *Can. J. Phys.* **58**, 1356 (1980).
13. M. Okumura, M. -C. Chan, and T. Oka, *Phys. Rev. Lett.* **62**,32 (1989).
14. M. -C. Chan, M. Okumura, C. M. Gabrys, L.-W. Xu, B. D. Rehfuss, and T. Oka, *Phys. Rev. Lett.* **66**, 2060 (1991).

15. R. A. Steinhoff, K. V. S. R. Apparao, D. W. Ferguson. K. N. Rao, B. P. Winnewisser, and M. Winnewisser, *Can. J. Phys.* **72**, 1122 (1994).

16. M. -C. Chan, L.-W. Xu, C. M. Gabrys, and T. Oka, *J. Chem. Phys.* **95**, 9404 (1991).

17. D. P. Weliky, K. E. Kerr, T. J. Byers, Y. Zhang, T. Momose, and T. Oka, J. *Chem. Phys.* **105**, 4461 (1996).

18. M. -C. Chan,, *PhD thesis.* Univ.Chicago, Chicago, Ill. (1991)

19. T. Momose, *J. Chem. Phys.* **107**, 7695 (1997).

20. T. Momose, M. Miki, T. Wakabayashi, T. Shida, M. -C. Chan, S. S. Lee, and T. Oka, *J. Chem. Phys.* **107**, 7707 (1997).

21. T. Momose, H. Katsuki, H. Hoshina, N. Sogoshi, T. Wakabayashi, and T. Shida, *J. Chem. Phys.* **107**, 7717 (1997).

22. M. -C. Chan, M. Okumura, and T. Oka, *J. Phys. Chem. A*, **104**, 3775 (2000)

23. T. Oka, *Phys. Rev. Lett.* **34**, 4795 (2001)

24. J. Van Kranendonk, *Solid Hydrogen, Theory of the Properties of Solid H_2, HD, and D_2* (Plenum Press, New York, 1983).

25. G. Gales, M. F. Libert, R. Sellier, L. Cournac, V. Chapon, and T. Heulin, *FEMS Microbiol Lett.* **240(2)**, 155 (2004)

26. R. Y. Morita, *Microbial Ecology* , **38(4)**, 307 (1999)

27. B. Bogdanovic, and M. Schwickardi, *Applied Physics*, **A 72**, 221 (2001)

28. M. Ritschel, M. Uhlemann, et.al., *App. Phys. Lett.* **80**, 2987 (2002)

29. R. B. Scott, *Cryogenic Engineering*, Met-Chem Research, Boulder, CO, (1959).

30. R. G. Bohn and C. F. Mate, *Phys. Rev. B*, **2**, 2121 (1970).

31. H. M. Roder, G. E. Childs, R. D. McCarty and P. E. Angerhofer, NBS Technical Note 641, (1973).

32. H. W. Wooley, R. B. Scott, and F. G. Brickwedde, *J. Research NBS*, **41**, 379 (1948).

33. Y. E. Stetsenko, D. N. Bol'shutkin, and L. A. Indan, *Sov. Phys. Solid State*, **12**, 2958 (1971).

34. L. Pauling, *Phys. Rev.* **86**, 21 (1930).

35. M.-C. Chan, S. S. Lee, M. Okumura, and T. Oka, *J. Chem. Phys.* **95**, 88 (1991).

36. R. M. Dickson and T. Oka, *Phys. Rev. B*, **57**, 950 (1998)

37. V. F. Sears and J. Van Kranendonk, *Can. J. Phys.* **42**, 980 (1964).

38. S. Luryi and J. Van Kranendonk, *Can. J. Phys.* **57**, 307 (1979).

39. W. G. Moffatt, G. W. Pearsall and J. Wulff, *Structure and Properties of Materials, Vol .I, Strcuture*, (New York , Wiley, 1966)

40. T. Oka, *Annu. Rev. Phys. Chem.* **44**, 29 (1993) and references therein.

41. L. H. Nosanow, *Phys. Rev.* **146**, 120 (1966)

42. A. Van Orden, and R. J. Saykally, *Chem. Rev.* **98**, 2313 (1998).

43. P. C. Souers, *Hydrogen Properties for Fusion Energy* (University of California Press, Berkeley, 1986).

44. I. F. Silvera, *Rev. Mod. Phys.* **52**, 393 (1980).

45. J. C. McLennan and J. H. McLeod, *Nature* **123**, 160 (1929).

46. E. J. Allin, W. F. J. Hare, and R. E. MacDonald, *Phys. Rev.* **98**, 554 (1955).

47. D. P. Weliky, T. J. Byers, K. E. Kerr, T. Momose, R. M. Dickson, and T. Oka, *Appl. Phys. B* **59**, 265 (1994).

48. T. Momose, D. P. Weliky, and T. Oka, *J. Mol. Spectrosc.* **153**, 760 (1992).

49. R. M. Dickson, T. J. Byers, and T. Oka, *J. Low Temp. Phys.* **102**, 241 (1996).

50. Y. Zhang, T. J. Byers, M.-C. Chan, T.Momose, K. E. Kerr, D. P. Weliky, and T. Oka, *Phys. Rev. B* **58**, 1 (1998)

51. E. Goovaerts, X. Y. Chen, A. Bouwen, and D. Schoemaker, *Phys. Rev. Lett.* **57**, 479 (1986).

52. G. Herzberg, *Molecular Spectra and Molcular Structure I. Spectra of Diatomic Molecules*, 2nd ed. (Litton Educational Publishing, Inc., New York, 1950).

53. P. R. Bunker and P. Jensen, *Molecular Symmetry and Spectroscopy*, 2nd ed. (NRC Research Press, Ottawa, Ontario, Canada. 1998)

54. R. S. Mulliken, *Phys. Rev.*, **43**, 279 (1933)

55. J. T. Hougen, *J. Chem. Phys.* **37**, 1433 (1962).

56. H. C. Longuet-Higgins, *Mol. Phys.* **6**, 445 (1963).

57. R. E. Miller and J. C. Decius, *J. Chem. Phys.* **59**, 4871 (1973).

58. L. D. Landau and E. M. Lifshitz, *Quantum Mechanics: Non-Relativistic Theory*, 3rd ed, (Pergamon, New York. 1977).

59. W. Kolos and L. Wolniewicz. *Rev. Mod. Phys.* **35**, 473 (1963)

60. J. I. Steinfeld, *Molecules and Radiation*, (MIT Press, 1989)

61. H. M. Hulburt and J. O. Hirschfelder, *J. Chem. Phys.* **9**, 61 (1940).

62. E. Steele, E. R. Lippincott and J. T. Vanderslice, *Rev. Mod. Phys.* **34**, 239 (1962).

63. S. M. Kirschner, R. J. Le Roy, J. F. Ogilvie, and R. H. Tipping, *J. Mol. Spectrosc.* **65**, 306 (1977).

64. J. M. Hure and E. Roueff, *J. Mol. Spectrosc.* **160**, 335 (1993).

65. D. G. Truhlar, *Inter. J. Quan. Chem.* **VI**, 975 (1972).

66. R. K. Nesbet, *J. Chem Phys.* **40**, 3619 (1964).

67. W. M. Huo, *J. Chem. Phys.* **43**, 624 (1955).

68. J. S. Muenter, *J. Mol. Spectrosc.* **55**, 490 (1975).

69. T. Kihara and S. Koba, *J. Phys. Soc. (Japan)* **7**, 348 (1952).

70. A. B. Harris, *Phys. Rev. B*, **1**, 1881 (1970).

71. V. B. Koshenev, *Sov. J. Low. Temp. Phys.* **2**, 118 (1976).

72. E. K. Plyler, , L. R. Blaine and W. S. Connor, *J. Opt. Soc. Amer.*, **45**, 102 (1955).